Journal of Alloys and Compounds 509 (2011) 5177–5182

Contents lists available at ScienceDirect

Journal of Alloys and Compounds

journal homepage: www.elsevier.com/locate/jallcom

Tetragonal-cubic phase boundary in nanocrystalline ZrO_2–Y_2O_3 solid solutions synthesized by gel-combustion

Ismael O. Fábregas[a], Aldo F. Craievich[b], Márcia C.A. Fantini[b], Ricardo P. Millen[c], Márcia L.A. Temperini[c], Diego G. Lamas[a,d,*]

[a] CINSO (Centro de Investigaciones en Sólidos), CITEFA-CONICET, J.B. de La Salle 4397, 1603 Villa Martelli, Pcia. de Buenos Aires, Argentina
[b] Instituto de Física, Universidade de São Paulo, Travessa R da Rua do Matão, No. 187, Cidade Universitaria, 05508-900 São Paulo, Brazil
[c] Instituto de Química, Universidade de São Paulo, Avenida Prof. Lineu Prestes 748, Cidade Universitaria, 05508-900 São Paulo, Brazil
[d] Laboratorio de Caracterización de Materiales, Facultad de Ingeniería, Universidad Nacional del Comahue, Buenos Aires 1400, (8300) Neuquén Capital, Prov. de Neuquén, Argentina

ARTICLE INFO

Article history:
Received 24 December 2010
Accepted 22 January 2011
Available online 2 March 2011

Keywords:
Nanostructured materials
Oxide materials
Crystal structure
Synchrotron radiation
X-ray diffraction

ABSTRACT

By means of synchrotron X-ray powder diffraction (SXPD) and Raman spectroscopy, we have detected, in a series of nanocrystalline and compositionally homogeneous ZrO_2–Y_2O_3 solid solutions, the presence at room temperature of three different phases depending on Y_2O_3 content, namely two tetragonal forms and the cubic phase. The studied materials, with average crystallite sizes within the range 7–10 nm, were synthesized by a nitrate–citrate gel-combustion process. The crystal structure of these phases was also investigated by SXPD. The results presented here indicate that the studied nanocrystalline ZrO_2–Y_2O_3 solid solutions exhibit the same phases reported in the literature for compositionally homogeneous materials containing larger (micro)crystals. The compositional boundaries between both tetragonal forms and between tetragonal and cubic phases were also determined.

1. Introduction

Zirconia-based ceramics are intensely investigated because of their excellent electric and mechanical properties. In particular, TZP ('tetragonal zirconia polycrystals') ceramics exhibit high ionic conductivity at intermediate temperatures and high fracture toughness [1,2]. These ceramics are used in many applications, mainly in electrochemical devices such as oxygen sensors, oxygen pumps, and solid-oxide fuel cells [3].

Pure, undoped zirconia presents three stable phases that depend on temperature: monoclinic (stable below 1473 K), tetragonal (stable between 1473 and 2553 K) and cubic (stable from 2533 K up to the melting point at 2988 K) [1,2]. Unfortunately, only the high temperature tetragonal and cubic phases have adequate properties for technological applications. The cubic polymorph can be fully stabilized at room temperature by introducing dopants such as Y_2O_3, CaO, MgO, and CeO_2. In contrast, the tetragonal phase cannot be stabilized in all these systems, being the monoclinic phase the thermodynamically stable polymorph at room temperature. However, it has been found that the tetragonal phase can be retained in nanocrystalline powders and fine-grained ceramics [2].

For compositionally homogeneous ZrO_2-based materials, the existence of three tetragonal forms, known as t, t′ and t″, all belonging to the $P4_2/nmc$ space group have been reported [4–13]. The t-form is the stable one, limited to the solubility limit predicted by the equilibrium phase diagram. The dopant oxides exhibit a wider solubility range in the t′-form, which is unstable against the mixture of the t-form and cubic phase. The t″-form – that can be retained for high dopant contents – has a c/a ratio of unity, but the oxygen atoms are displaced along the c-axis from their ideal sites in the cubic phase (8c sites of the space group). Finally, the cubic phase having a fluorite-type structure ($Fm\bar{3}m$ space group) is fully stabilized for even higher dopant concentration.

Yashima et al. [4–9] investigated the conditions for retention of metastable tetragonal forms, at room temperature, in compositionally homogeneous ZrO_2-based solid solutions for several systems composed of coarse (micro) crystals. In the case of ZrO_2–Y_2O_3 solid solutions, these authors have carefully characterized compositionally homogeneous powders synthesized by arc melting and rapid quenching [4,6,7] or by solid-state reaction [5]. Yashima and coworkers established that the t′/t″ and t″/cubic compositional boundaries are located around 9 and 11 mol% Y_2O_3, respectively. They also established the presence of a mixture of t′ and t″ for a solid solution with composition of ZrO_2-14 mol% $YO_{1.5}$ (ZrO_2-7.5 mol% Y_2O_3) [5].

* Corresponding author at: Universidad Nacional del Comahue - Facultad de Ingeniería, Laboratorio de Caracterización de Materiales, Buenos Aires 1400, (8300) Neuquén capital, Provincia de Neuquén, Argentina.
E-mail addresses: dlamas@uncoma.edu.ar, diego_german_lamas@yahoo.com.ar, dlamas@citefa.gov.ar (D.G. Lamas).

0925-8388/$ – see front matter © 2011 Elsevier B.V. All rights reserved.
doi:10.1016/j.jallcom.2011.01.213

In the last few years, we have investigated the presence of metastable tetragonal forms in compositionally homogeneous ZrO_2-based solid solutions composed of small nanocrystals, instead of microcrystalline materials as studied by Yashima and coworkers. The studied nanocrystalline solid solutions were synthesized by gel-combustion routes [10–14]. Interestingly, we have demonstrated that similar tetragonal forms can be retained in nanocrystalline ZrO_2–Y_2O_3 [10], ZrO_2–CeO_2 [11,12], ZrO_2–CaO [13] and ZrO_2–Sc_2O_3 [14] systems, but the lattice parameters, axial ratio and oxygen displacement may change with the crystallite size and/or synthesis route.

In a previous work [10], we investigated nanocrystalline ZrO_2–Y_2O_3 solid solutions by powder diffraction using a conventional X-ray source (XPD). From these data, the lattice parameters and the position of oxide anions in the tetragonal cell could not be precisely determined. Moreover, the t″/cubic compositional boundary was not established. In order to more precisely determine the compositional dependence of the crystal structure of the nanocrystalline solid solutions and establish the t″/cubic boundary, a new study of compositionally homogeneous ZrO_2-4 to 12 mol% Y_2O_3 nanopowders using synchrotron X-ray powder diffraction (SXPD) and Raman spectroscopy was performed.

As we will see, the techniques used here, SXPD and Raman spectroscopy, allowed us a precise analysis of the phase diagram and crystal structure of our nanocrystalline ZrO_2–Y_2O_3 solid solutions. In particular, the measurement of the weak 1 1 2 X-ray reflection corresponding to the tetragonal phase – a forbidden reflection in the cubic fluorite structure – provided an accurate determination of the oxygen positions in the unit cell. Besides, in contrast to our previous work [10], both techniques made possible to distinguish between the tetragonal t″-form and the cubic phase and, therefore, determine the t″/cubic compositional boundary, a result that completes the whole phase diagram of nanocrystalline ZrO_2–Y_2O_3 solid solutions.

2. Experimental procedure

2.1. Synthesis of nanocrystalline ZrO_2–Y_2O_3 solid solutions

Nanocrystalline ZrO_2-4, 6, 7, 8, 9, 10, 11 and 12 mol% Y_2O_3 nanopowders were synthesized by a pH-controlled nitrate–citrate gel-combustion process previously developed by the authors [10,15,16]. $ZrOCl_2{\cdot}8H_2O$ (Alpha Aesar, USA, 99.9%) and Y_2O_3 (GFS company, UK, 99.99%) were used as raw compounds.

A final calcination procedure at 600 °C for 2 h was performed in order to remove the organic residues.

2.2. Synchrotron X-ray powder diffraction (SXPD)

SXPD experiments were carried out using the D12A-XRD1 beamline of the Brazilian Synchrotron Light Laboratory (LNLS, Campinas, Brazil). In order to detect the rather weak 1 1 2 Bragg reflection, a high-intensity, low-resolution ($\Delta d/d = 0.0015$, $2\theta = 90°$) configuration, without crystal analyzer, was used [12]. The wavelength was set at 1.50008 Å. Data in the angular region of $2\theta = 20$–$130°$ were collected in step-scanning mode, with a step of 0.05° and a counting time of 3 s/step.

The crystallite size of all the solid solutions was determined from the full-width at half-maximum of the 1 1 1 peak by means of the Scherrer equation [17], considering the instrumental broadening determined from the analysis of a LaB_6 standard (NIST-SRM 660a).

2.2.1. Rietveld analysis

Rietveld refinements were performed using the *FullProf* code [18]. We followed the same procedure utilized in our previous work on the ZrO_2–CeO_2 system [12].

For the tetragonal phase, the $P4_2/nmc$ space group was assumed, with (Zr^{4+};Y^{3+}) cations and O^{2-} anions in 2a and 4d positions, respectively. The results of these refinements are given in terms of the usual pseudo-fluorite unit cell. In the case of the cubic phase (with a fluorite-type structure), the $Fm\bar{3}m$ space group was considered, with (Zr^{4+};Y^{3+}) cations and O^{2-} anions in 4a and 8c positions, respectively. The peak shape was assumed to be a pseudo-Voigt function in both cases. The background of each profile was adjusted by a six-parameter polynomial function in $(2\theta)^n$, $n = 0$–5. Isotropic atomic temperature parameters were used. The thermal parameters corresponding to Zr^{4+} and Y^{3+} atoms were assumed to be equal.

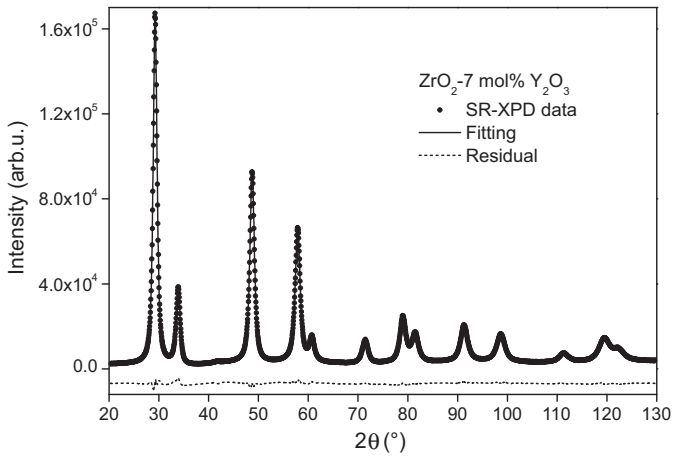

Fig. 1. Experimental SXPD data and fit obtained after Rietveld refinement assuming one tetragonal phase for the ZrO_2-7 mol% Y_2O_3 sample.

2.2.2. Direct determination of the position of O^{2-} anions in the tetragonal phase

In the cubic phase, O^{2-} anions are in (¼ ¼ ¼) and equivalent positions, while in the tetragonal phase they are displaced along the *c*-axis. The fractional *z*-coordinate of O^{2-} anion in the asymmetric unit, $z_{(O)}$, can be derived from the ratio of the intensities of the 1 1 2 and 1 1 1 peaks, I(1 1 2) and I(1 1 1), respectively. The 1 1 2 reflection is only related to the position of O^{2-} anions, while the 1 1 1 one is only related to the Zr^{4+} and Y^{3+} cations, as can be easily demonstrated by calculating the corresponding structure factors. The $z_{(O)}$ value is related to the I(1 1 2)/I(1 1 1) ratio by the following equation [12,13],

$$\frac{I(1\ 1\ 2)}{I(1\ 1\ 1)} = \frac{4 f_O^2 \sin^2(4\pi z_{(O)}) q_O{}^2 L_{1\,1\,2}}{f_{Zr\text{-}Y}^2 q_{Zr\text{-}Y}^2 L_{1\,1\,1}} \quad (1)$$

where $f_{Zr\text{-}Y}$ is the average atomic scattering factor of Zr^{4+} and Y^{3+} cations, $q_{Zr\text{-}Y}$, is their average temperature factor, f_O is the atomic scattering factor of O^{2-} anion, q_O is its temperature factor, and $L_{1\,1\,2}$ and $L_{1\,1\,1}$ are the Lorentz factors corresponding to the 1 1 2 and 1 1 1 peaks (for a symmetric θ–2θ scan, $L(\theta) = \cos(\theta)/\sin 2(2\theta)$).

The displacement of O^{2-} anions from their positions in the cubic phase, $d_{(O)}$, can be easily determined by the equation:

$$d_{(O)} = \left(\tfrac{1}{4} - z_{(O)}\right) * c \quad (2)$$

where *c* is the lattice constant in the *c* direction.

2.3. Raman spectroscopy

Raman spectra were recorded in a Renishaw Imaging Microscope System 3000 spectrophotometer equipped with an Olympus BH-2 microscope and a CCD detector. A 632.8 nm He–Ne laser line (Spectra Physics, model 127) was used as excitation radiation and the laser power at the sample was 1.8 mW. Spectra acquisition consisted of 5 scans of 20 s duration each.

3. Results and discussion

3.1. Compositional boundary between the tetragonal t′-form (tetragonal unit cell) and the tetragonal t″-form (cubic unit cell)

Fig. 1 displays the whole diffraction pattern corresponding to the ZrO_2-7 mol% Y_2O_3 solid solution. This pattern was well fitted by Rietveld procedure by assuming the presence of only one phase, namely the tetragonal t′-form. All the other SXPD patterns were also indexed and well fitted by assuming, in all cases, a single-phased material with one of the tetragonal forms or the cubic phase, depending on composition. No evidence of a mixture of phases was detected, as confirmed by a careful study of the SXPD data and the Rietveld fitted profile. The average crystallite sizes of the studied set of solid solutions, listed in Table 1, were within the 7–10 nm range.

The lattice parameters derived from Rietveld refinements are reported in Table 2 and Fig. 2a. They slightly differ from those reported in our preliminary work using classical XPD [10]. This could be due to the use of chemical reagents purchased from

Table 1
Average crystallite size of all the nanocrystalline ZrO_2–Y_2O_3 powders studied in this work, as determined by the Scherrer equation.

Y_2O_3 content (mol%)	D (nm)
4	8.1 (5)
6	8.0 (5)
7	8.7 (5)
8	8.7 (5)
9	9.6 (5)
10	10 (1)
11	7.0 (5)
12	7.3 (5)

different commercial companies, which may affect the composition of the resulting material. Anyway, the lattice parameters that we determined here are expected to be more precise than those reported in reference [10] because, in the present work, (i) we studied samples synthesized from higher purity reagents and (ii) we have determined the SXPD patterns using a high-intensity configuration thus providing experimental results with much better statistics than using the classical XPD technique.

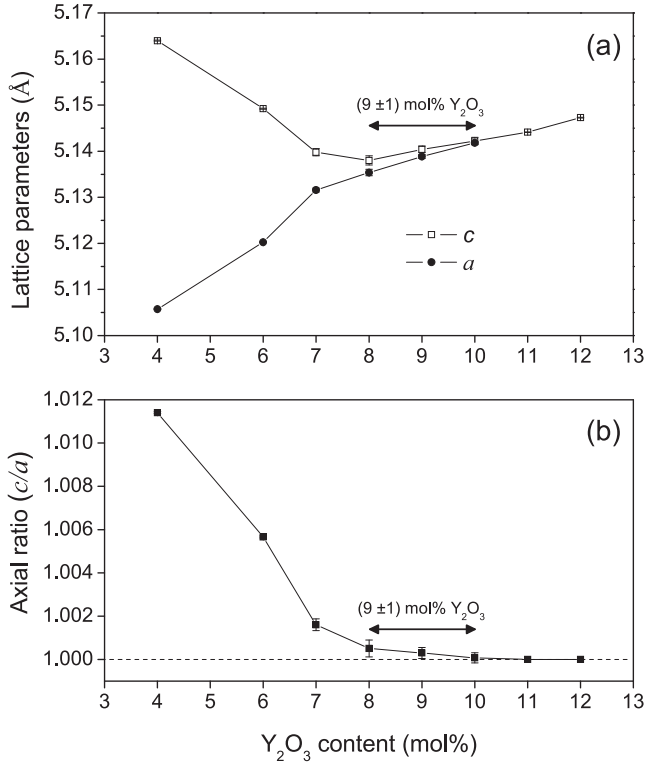

Fig. 2. Variation of the lattice parameters, a and c, and the axial ratio, c/a, as functions of Y_2O_3 content. The t′/t″ compositional boundary at (9 ± 1) mol% Y_2O_3 is indicated with arrows.

The ratio (c/a) determined from the lattice parameters a and c derived from Rietveld fittings are plotted in Fig. 2b. This ratio decreases for increasing Y_2O_3 content and becomes unity at 10 mol% Y_2O_3. Therefore, we have firstly concluded that the compositional boundary t′ ($c/a > 1$)/t″ ($c/a = 1$) is located at (9.5 ± 0.5) mol% Y_2O_3. However, we noticed that for 9 mol% Y_2O_3 the value of c/a is only slightly higher than 1 (approximately within the error bar as it can be seen in Fig. 2b). Therefore, we concluded that a more realistic composition for the t′/t″ phase boundary is (9 ± 1) mol% Y_2O_3.

The lattice parameters determined here for nanocrystalline powders are slightly different from those reported by Yashima et al. for microcrystalline materials. Besides, the axial ratios c/a of our t′ samples are smaller than those reported by these authors. This is a qualitatively expected result because it is well-known that, for smaller crystallite sizes, the crystal structure approaches to the cubic fluorite-type structure [19].

The isotropic temperature factors of cations and anions, $B_{(Zr\text{-}Y)}$ and $B_{(O)}$, are presented in Table 2. Both parameters increase with increasing Y_2O_3 content. These increasing trends are attributed to the distortion generated by the introduction of Y in the solid solutions [20].

3.2. Compositional boundary between the tetragonal t″-form (cubic unit cell) and the cubic phase

3.2.1. SXPD

The t″/c phase boundary was determined using SXPD data by analyzing the profile of *h k l* Bragg peaks that are expected to appear in the diffraction patterns for the tetragonal forms and, on the contrary, vanish for the cubic phase. This study could not be performed by Rietveld analysis described in the precedent section because these Bragg peaks are extremely weak and thus their weight in any global analysis of the diffraction pattern is very small.

For the purpose of quantitatively determining the compositional boundary t″/c, we have selected the 1 1 2 Bragg peak, which is "forbidden" for cubic fluorite-like structures. In order to improve statistics, data close to the 1 1 2 reflection were collected using long step-counting times. The SXPD profiles are plotted in Fig. 3. The 1 1 2 peak was detected for Y_2O_3 content from 4 up to 10 mol% Y_2O_3, thus indicating that these samples exhibited the tetragonal phase. Above this composition, the 1 1 2 peak vanished. Fig. 4a displays the integrated intensity of the 1 1 2 reflection, I(1 1 2), as a function of Y_2O_3 content, showing that I(1 1 2) vanishes at (10.5 ± 0.5) mol%, which corresponds to the tetragonal(t″-form)/cubic phase boundary.

Fig. 4b and 4c show the $z_{(O)}$ coordinate of the O^{2-} anion in the asymmetric unit of the tetragonal unit cell and its distance $d_{(O)}$ from its position in the cubic fluorite-like structure, respectively, as functions of Y_2O_3 content. The values of $z_{(O)}$ and $d_{(O)}$ determined using equations (1) and (2) are also reported in Table 3. The $z_{(O)}$ coordinate tends to ¼ for increasing Y_2O_3 content, as expected for this transition. The oxygen displacement, $d_{(O)}$, decreases for increas-

Table 2
Structural parameters determined by Rietveld analysis and standard Rietveld agreement factors obtained for all nanocrystalline ZrO_2–Y_2O_3 solid solutions studied in this work. a and c are the lattice parameters, c/a is axial ratio, $B_{(Zr;Y)}$ and $B_{(O)}$ are the isotropic temperature factors and R_p, R_{wp} and R_{exp} are the standard Rietveld agreement factors.

	4 mol% Y_2O_3 $P4_2/nmc$	6 mol% Y_2O_3 $P4_2/nmc$	7 mol% Y_2O_3 $P4_2/nmc$	8 mol% Y_2O_3 $P4_2/nmc$	9 mol% Y_2O_3 $P4_2/nmc$	10 mol% Y_2O_3 $P4_2/nmc$	11 mol% Y_2O_3 $Fm\bar{3}m$	12 mol% Y_2O_3 $Fm\bar{3}m$
a (Å)	5.1058(1)	5.1202(1)	5.1316(4)	5.1354(7)	5.1388(4)	5.1436(3)	5.1441(1)	5.1473(1)
c (Å)	5.1641(2)	5.1492(4)	5.1398(8)	5.1380(9)	5.1404(7)	5.1444(8)		
c/a	1.01143(7)	1.0057(1)	1.0016(2)	1.0005(3)	1.0003(2)	1.0002(2)	1	1
$B_{(Zr;Y)}$ (Å^2)	0.52(2)	0.62(2)	0.74(1)	0.71(1)	0.80(1)	0.91(1)	0.99(1)	0.99(2)
$B_{(O)}$ (Å^2)	1.50(7)	1.83(7)	1.75(7)	1.71(7)	2.08(7)	2.37(8)	2.37(8)	2.89(7)
R_p	3.96	3.92	4.23	4.73	4.98	5.46	6.380	6.17
R_{wp}	5.44	5.4	5.73	6.21	6.39	6.9	7.9	7.74
R_{exp}	2.93	2.88	1.3	1.25	1.27	1.23	1.3	1.27

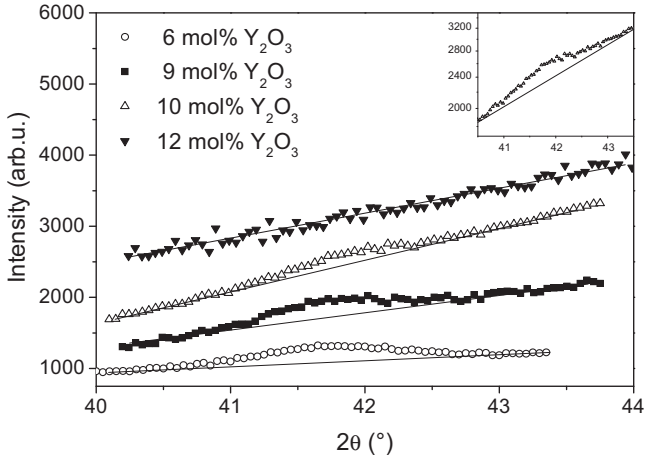

Fig. 3. SXPD data close to the 1 1 2 Bragg reflection for the ZrO_2-6, 9, 10 and 12 mol% Y_2O_3 solid solutions, taken with step-counting times of 12 s, 15 s, 30 s and 30 s, respectively. All data were normalized considering these different step-counting times. The inset shows the ZrO_2-10 mol% Y_2O_3 sample in more detail. The straight lines are a guide for the visualization of the background.

ing Y_2O_3 content and vanishes at a composition between 10 and 11 mol% Y_2O_3, thus confirming the tetragonal(t″-form)/cubic phase boundary indicated above.

3.2.2. Raman spectroscopy

In order to confirm the compositional domain of the tetragonal t″ and cubic phases derived from X-ray diffraction analysis, Raman spectroscopy was applied. Group theory predicts six Raman-active modes (one A_{1g}, three E_g and two B_{1g} modes) for the ZrO_2 or ZrO_2-based tetragonal phase, while the cubic phase only exhibits one F_{2g} Raman-active mode [4,21]. It has also been reported that some modes of the tetragonal phase are not detected for the t″-form [4].

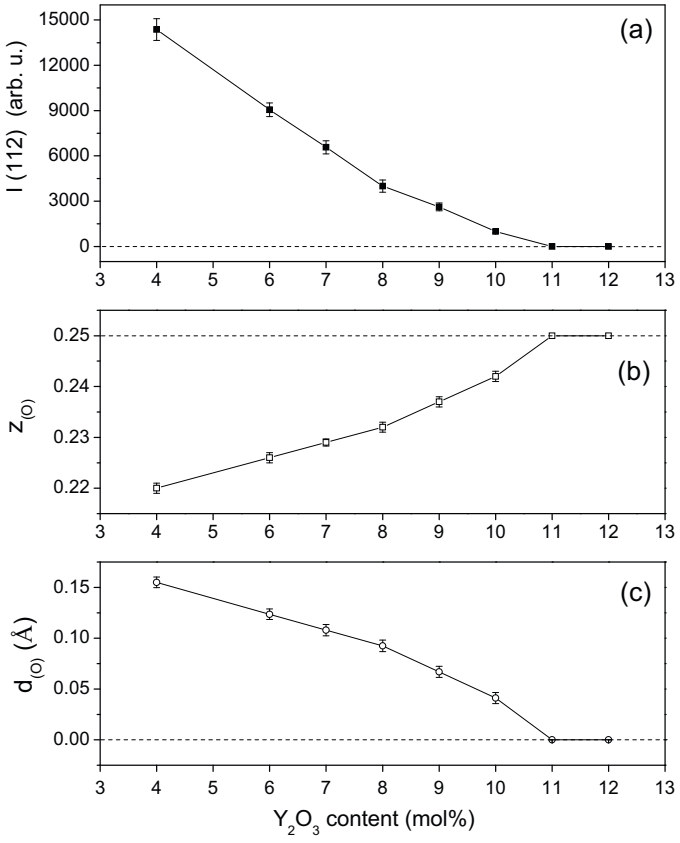

Fig. 4. (a) Integrated intensity of the 1 1 2 Bragg reflection, (b) $z_{(O)}$ fractional coordinate and (c) $d_{(O)}$ distance, as functions of Y_2O_3 content. See text for details.

Table 3
Fractional *z*-coordinate of O^{2-} anion in the asymmetric unit, $z_{(O)}$, determined from the I(1 1 2)/I(1 1 1) ratio and displacement of O^{2-} anions from their positions in the cubic phase, $d_{(O)}$.

Y_2O_3 content (mol%)	$z_{(O)}$	$d_{(O)}$ (Å)
4	0.220(1)	0.155(5)
6	0.221(1)	0.124(5)
7	0.229(1)	0.108(6)
8	0.232(1)	0.092(6)
9	0.237(1)	0.067(5)
10	0.242(1)	0.041(5)
11	0.250	0
12	0.250	0

Raman spectra for different nanocrystalline ZrO_2–Y_2O_3 solid solutions are plotted in Fig. 5. The five expected bands for a tetragonal phase for the wavenumber range studied in this work are numbered from 2 to 6 following the notation of Yashima et al. [4], since the first mode at about 150 nm^{-1} was not recorded within the range of wavelength number of our measurements. Band 6 is the only band that is expected to appear for a cubic phase. Five bands are apparent in the curves corresponding to compositions from ZrO_2-4 mol% Y_2O_3 up to 10 mol% Y_2O_3. As Y_2O_3 content increases, the intensities of Raman bands 2–6 decrease, with their positions varying continuously and vanishing in the spectra corresponding to 11 mol% Y_2O_3 content. At and above this composition, the Raman spectra exhibit a single band (6) corresponding to the F_{2g} mode of the cubic phase, at about 600 cm^{-1}. Band positions resulted in good agreement with those reported by Yashima et al. for ZrO_2–Y_2O_3 solid solutions with similar compositions [4].

Yashima et al. demonstrated that the height ratio between the fourth and sixth modes, I4/I6, is related to oxygen displacement from its position in the cubic fluorite-type unit cell [4]. Fig. 6 displays this ratio, which exhibits a monotonous decrease with composition and became zero between 10 and 11 mol% Y_2O_3. This result indicates that the t″/c transition in nanocrystalline ZrO_2–Y_2O_3 solid solutions occurs at (10.5 ± 0.5) mol% Y_2O_3, in good agreement with the value independently determined by the above SXPD analysis following the intensity of the 1 1 2 Bragg peak and with the previous results reported by Yashima et al. for microcrystalline solid solutions.

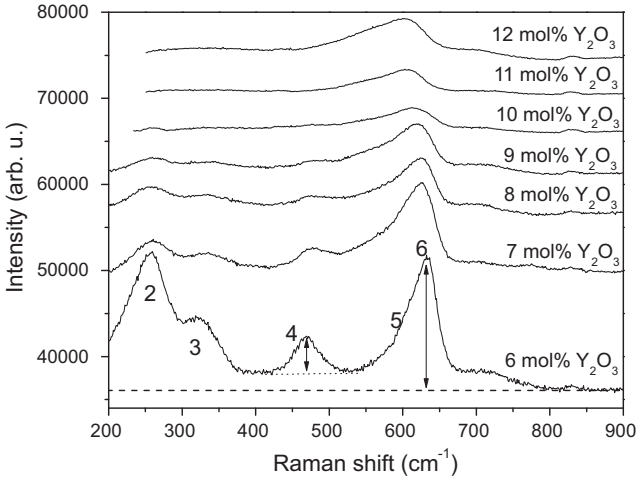

Fig. 5. Raman spectra of ZrO_2–Y_2O_3 solid solutions. The numbers correspond to the bands mentioned in the text and in Ref. [4]. The dotted line is the background estimation for the forth band while the dashed line corresponds to the sixth one.

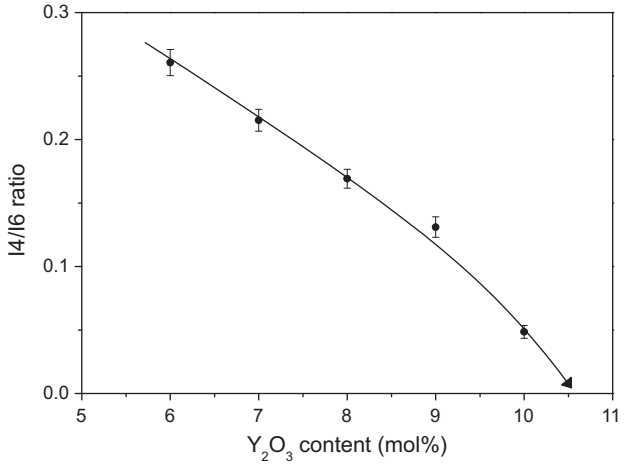

Fig. 6. I4/I6 peak height ratio derived from Raman spectroscopy analysis, as functions of Y_2O_3 content. The solid line is a guide to the eye.

3.3. Comments about the homogeneous nature of the nanocrystalline ZrO_2–Y_2O_3 powders synthesized by gel-combustion

Fig. 7 displays the so called pseudo-cubic lattice parameter, defined as $a^* = (2a + c)/3$, as a function of Y_2O_3 content. As predicted by Vegard's law [22], a clearly linear behavior is observed over the whole composition range, thus confirming the compositionally homogeneous nature of the solid solutions prepared by the gel-combustion procedure [10–14,23–29]. The compositional homogeneity of materials synthesized by gel-combustion routes can be explained considering that the system remains homogeneous during the whole process and the final combustion step of the precursor gel proceeds very rapidly, thus preserving the compositional homogeneity in the as-reacted material.

Yashima et al. [5] discovered that microcrystalline powders with a composition ZrO_2-14 mol% $YO_{1.5}$ (ZrO_2-7.5 mol% Y_2O_3) exhibit a mixture (t′ and t″) of phases. On the other hand, these authors have also established that ZrO_2-12 mol% $YO_{1.5}$ (ZrO_2-6.4 mol% Y_2O_3) and ZrO_2-16 mol% $YO_{1.5}$ (ZrO_2-8.7 mol% Y_2O_3) are single-phased. These results indicate the presence of a rather narrow two-phase gap in the phase diagram close to ZrO_2-7.5 mol% Y_2O_3. Since we have only studied powders with Y_2O_3 contents of 7.0 and 8.0 mol% Y_2O_3, we could not confirm the eventual presence of the same narrow two-phase domain in nanocrystalline materials. Taking into account that we did not have any experimental evidence for the existence of a mixture of phases, we have not consider the possible existence of t′/t′ + t″ and t′ + t″/t″ compositional boundaries in our nanocrystalline powders. However, further investigation for compositions between 7 and 8 mol% Y_2O_3 should be performed to address this issue.

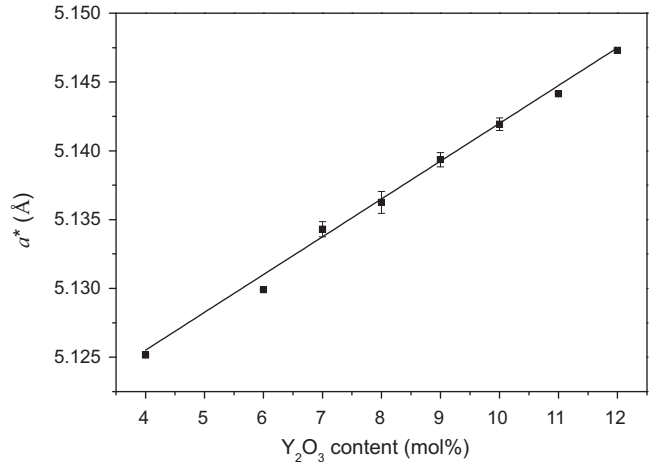

Fig. 7. Pseudo-cubic lattice parameter, $a^* = (2a + c)/3$, as a function of Y_2O_3 content. The solid line is a linear fit of the experimental results.

4. Conclusions

We have analyzed the crystal structure of nanocrystalline and compositionally homogeneous ZrO_2–Y_2O_3 solid solutions synthesized by a gel-combustion process and identified the presence at room temperature of the metastable forms of the tetragonal phase, t′ and t″, and the stable cubic phase in these powdered materials.

The t′/t″ compositional boundary determined in this work for nanocrystalline ZrO_2–Y_2O_3 solid solutions using Rietveld refinements of SXPD data was (9 ± 1) mol% Y_2O_3, in good agreement with the value established in a previous investigation of nanocrystalline powders [10] and also with the result reported by Yashima et al. [4–7] for materials composed of larger (micrometric) crystallites synthesized by arc melting and rapid quenching or by solid-state reaction [4–7]. However, the c/a ratios for the t′-form reported here are slightly smaller those determined by Yashima et al. [4–7].

The tetragonal t″/cubic boundary, which was not established in our previous work by conventional XPD [10], was determined in the present work by SXPD following one of the "forbidden" Bragg reflections and also by Raman spectroscopy. Both techniques yielded the same t″/cubic compositional boundary, namely (10.5 ± 0.5) mol% Y_2O_3. Again, this result is in good agreement with that reported by Yashima et al. [4–7], thus indicating that nanocrystalline and microcrystalline compositionally homogeneous ZrO_2–Y_2O_3 solid solutions exhibit similar crystallographic features.

Finally, for the whole series of nanocrystalline ZrO_2–Y_2O_3 solid solutions studied here, no evidences of the presence of a mixture of phases – as reported by Yashima et al. [4–7] for microcrystalline solid solutions – were detected.

Acknowledgements

The present work was performed within the frame of the scientific collaboration agreements CAPES-MinCyT and CNPq-CONICET between Brazil and Argentina. It was also partially supported by the Brazilian Synchrotron Light Laboratory (LNLS, Brazil, proposal D12A-XRD1-1857), CNPq (Brazil, PROSUL programs 490289/2005-3 and 490580/2008-4), Agencia Nacional de Promoción Científica y Tecnológica (Argentina, PICT 2005 No. 38309, PICT 2007 No. 01152 and PAE-PICT 2007 No. 02288), CONICET (Argentina, PIP No. 6559) and Latin-American Centre for Physics (CLAF).

References

[1] W.E. Lee, W.M. Rainforth, Ceramic Microstructures: Property Control by Processing, Chapman and Hall, London, 1994, 317.
[2] R.E. Juarez, D.G. Lamas, G.E. Lascalea, N.E. Walsöe de Reca, Diff. Defect Forum 177 (1999) 1.
[3] C. Deportes, M. Duclot, P. Fabry, J. Fouletier, A. Hammou, M. Kleitz, E. Siebert, J.L. Souquet, Electrochimie des Solides, Presses Universitaires de Grenoble, Grenoble, 1994.
[4] M. Yashima, K. Ohtake, H. Arashi, M. Kakihana, M. Yoshimura, J. Appl. Phys. 74 (1993) 7603.
[5] M. Yashima, S. Sasaki, M. Kakihana, Y. Yamaguchi, H. Arashi, M. Yoshimura, Acta Cryst. B 50 (1994) 663.
[6] M. Yashima, M. Kakihana, M. Yoshimura, Solid State Ionics 86–88 (1996) 1131.
[7] M. Yashima, K. Ohtake, M. Kakihana, H. Arashi, M. Yoshimura, J. Phys. Chem. Solids 57 (1996) 17.
[8] M. Yashima, M. Kakihana, K. Ishii, Y. Ikuma, M. Yoshimura, J. Mater. Res. 11 (1996) 1410.
[9] M. Yashima, S. Sasaki, Y. Yamaguchi, M. Kakihana, M. Yoshimura, T. Mori, Appl. Phys. Lett. 72 (1998) 182.

[10] D.G. Lamas, N.E. Walsöe de Reca, J. Mater. Sci. 35 (2000) 5563.
[11] D.G. Lamas, G.E. Lascalea, R.E. Juarez, E. Djurado, L. Perez, N.E. Walsöe de Reca, J. Mater. Chem. 13 (2003) 904.
[12] D.G. Lamas, R.O. Fuentes, I.O. Fábregas, M.E. Fernández de Rapp, G.E. Lascalea, J.R. Casanova, N.E. Walsöe de Reca, A.F. Craievich, J. Appl. Cryst. 38 (2005) 867.
[13] I.O. Fábregas, D.G. Lamas, N.E. Walsöe de Reca, M.C.A. Fantini, A.F. Craievich, R.J. Prado, J. Appl. Cryst. 41 (2008) 680.
[14] P.M. Abdala, A.F. Craievich, M.C.A. Fantini, M.L.A. Temperini, D.G. Lamas, J. Phys. Chem. C 113 (2009) 18661.
[15] D.G. Lamas, G.E. Lascalea, N.E. Walsöe de Reca, J. Eur. Ceram. Soc. 18 (1998) 1217.
[16] R.E. Juárez, D.G. Lamas, G.E. Lascalea, N.E. Walsöe de Reca, J. Eur. Ceram. Soc. 20 (2000) 133.
[17] H. Klug, L. Alexander, X-ray Diffraction Procedures for Polycrystalline and Amorphous Materials, Second ed., John Wiley and Sons, New York, 1974.
[18] J. Rodríguez-Carvajal, FullProf.98, version 0.2, Saclay, France, 1998.
[19] D.G. Lamas, A.M. Rosso, M. Suarez Anzorena, A. Fernández, M.G. Bellino, M.D. Cabezas, N.E. Walsöe de Reca, A.F. Craievich, Scripta Mater. 55 (2006) 553.
[20] P. Li, I.-W. Chen, J.E. Penner-Hahn, Phys. Rev. B 48 (1993) 10074.
[21] V.G. Keramidas, W.B. White, J. Am. Ceram. Soc. 57 (1974) 22.
[22] R. Di Monte, J. Kašpar, J. Mater. Chem. 15 (2005) 633.
[23] L.R. Pederson, G.D. Maupin, W.J. Weber, D.J. McReady, R.W. Stephens, Mater. Lett. 10 (1991) 437.
[24] N.A. Dhas, K.C. Patil, J. Mater. Sci. Lett. 12 (1993) 1844.
[25] K.R. Venkatachari, D. Huang, S.P. Ostrander, W.A. Schulze, G.C. Stangle, J. Mater. Res. 10 (1995) 748.
[26] A.K. Shukla, V. Sharma, N.A. Dhas, K.C. Patil, Mater. Sci. Eng. B 40 (1996) 153.
[27] D.G. Lamas, R.E. Juárez, G.E. Lascalea, N.E. Walsöe de Reca, J. Mater. Sci. Lett. 20 (2001) 1447.
[28] F. Zheng, R.K. Bordia, L.R. Pederson, Mater. Res. Bull. 39 (2004) 141.
[29] I.O. Fábregas, R.O. Fuentes, D.G. Lamas, M.E. Fernández de Rapp, N.E. Walsöe de Reca, M.C.A. Fantini, A.F. Craievich, R.P. Millen, M.L.A. Temperini, J. Phys: Condens. Matter. 18 (2006) 7863.